Desalination and Water Treatment
www.deswater.com
doi: 10.5004/dwt.2022.28442

260 (2022) 187–202
June

Selection of optimal performance characteristics during adsorption of Methyl red dye using sodium carbonate treated jute fibre

Amit Kumar Dey[a,*], Abhijit Dey[a], Rumi Goswami[a]

[a]*Department of Civil Engineering, Central Institute of Technology Kokrajhar, Assam-783370, India, Tel. +917002629867; email: ak.dey@cit.ac.in Orcid ID: 0000000340700231; Orcid ID: 0000000221267295; Orcid ID: 000000026662599X (A.K. Dey)*
[b]*Department of Mechanical Engineering, National Institute of Technology Srinagar, J&K-190006, India*

Received 2 November 2021; Accepted 27 March 2022

ABSTRACT

Use of Na_2CO_3 treated jute fibre (NTJF) for the removal of the azo dye Methyl red is described in this article. Face-centered CCD, based on response surface methodology experimental design, was used to obtain a specific number of experimental trails in order to improve experimentation and reach performance characteristics that are ideal for removing the Methyl red dye dissolved in aqueous solution. To investigate the impact of operating variables and their elucidation, an analysis of variance was used in conjunction with a second-order quadratic model. The computed and anticipated Q_e values were in resonance within the domain threshold with a desirability of 0.98, indicating exceptional accuracy of the experimentation operations. The following operating parameters were used for dye removal and equilibrium adsorption capacity (Q_e): Adsorbent (NTJF) dose, temperature, pH and rotational speed with Q_e of the treated jute being the performance measure for dye removal. Experimental results revealed that Langmuir isotherm was suitable, pseudo-second-order rate kinetic is better fitted, adsorption is endothermic in nature driven by chemisorption and there was high proximity between anticipated and experimental outcome of the research.

Keywords: Adsorption; Face cantered central composite second-order design (CCD); Response surface methodology (RSM); Na_2CO_3 treated jute fibre (NTJF); Methyl red

1. Introduction

In various industries, such as paper, textile, lather, plastic, food, cosmetics, and pharmaceuticals, excessive use of synthetic dyes to colour products has resulted in continuous discharge of dye contaminants into water bodies, causing water pollution. Several synthetic dyes have been linked to diseases such as cancer, asthma, and others [1]. Dyes are hazardous chemical substances that, when exposed to most objects, readily adhere to them and provide colour, as they do for cloth and fabrics. Furthermore, the textile industry alone consumes 100,000 tonnes/y, with approximately 100 tonnes of dye permitted to be discharged into bodies of water each year [2]. Because of their complex bonding structure, they are difficult to break, posing significant environmental and health risks. Certain dyes have been discovered to have mutagenic and carcinogenic properties, among other things [2]. Artificial dyes have been linked to serious side effects including hyperactivity in children, cancer, and allergies, according to numerous reports. However, this is a contentious topic, with researchers all over the world reporting contradictory findings [3,4]. The textile industry is the most common use of synthetic azo dyes [5]. Dye can be found in large quantities in textile industry effluents. Scientific research is focusing on the environmental and health risks associated with dye generated by textile businesses. As a result, environmental legislation is being enacted to regulate dye release, particularly azo-based dyes released directly into free-flowing water bodies. Depending on the

* Corresponding author.

approach, researchers have used a variety of techniques to effectively remove colour from wastewater bodies. Some of the procedures include membrane separation, biological oxidation treatment, coagulation–flocculation, ultrasonic irradiation, coagulation-flocculation, photocatalysis, and ozonation [6–12]. Among the various materials and methods, a combination of activated carbon (AC) and adsorption is one of the most effective ways to remove a large amount of dye from an aqueous solution in a practical manner. However, AC has its own set of drawbacks, such as a high initial manufacturing cost, difficulties with regeneration after depletion, and a reduction in removal effectiveness after regeneration [13,14]. As a result, today's researchers are emphasising the use of cost-effective, environmentally friendly, and abundant adsorbents [15–18]. In the present study the adsorption method was used to remove Methyl red (MR) dye from a low-cost bio-sorbent, Na_2CO_3 treated jute fibre (NTJF). Adsorption, regarded as one of the efficient techniques for the sequestration and cost effective adsorbents, has been considered as an excellent way for wastewater treatment [19].

Jute is an important crop on the Indian subcontinent, and it is one of India's many agricultural products. In India and Bangladesh, nearly 85% of the world's jute is produced. The main components of jute fibre are cellulose, hemicellulose, lignin, and other low-molecular-weight hydrocarbons [19]. The driving forces behind dye adsorption onto the adsorbent are these elements, which have hydroxyl and carboxyl functional groups. Apart from a high amount of α-cellulose (~60%), hemi-cellulose (~23%) and lignin (~14%) are the two other significant chemical elements found in jute, as well as traces of fat and wax. Researchers infers that an ester bond forms between sections of hemicellulose and lignin that are chemically linked by lignin's hydroxyl groups and hemicellulose's carboxyl groups [20]. The presence of carboxyl and hydroxyl groups on the outer surface of jute adsorbent is the primary cause for adsorption of dyes from aqueous media.

Researchers have successfully removed dye using several surface modified low-cost bio-sorbents, according to a literature review [21–23]. The focus has recently shifted to adsorbent surface modification in order to use it more effectively than activated carbon to remove hazardous colours from waste water. The goal of surface modification is to increase the percentages of important functional groups like sulphate, hydroxyl, carboxylate, carboxyl, and phosphate groups on the adsorbent surface [24]. When it comes to dye removal, researchers aren't limited to using only experimental models; there are a variety of mathematical models and software programmes that can be used to research and determine the ideal conditions for achieving the desired result. Several studies in this field have already been completed, such as the use of response surface methodology (RSM) to improve process factors for dye removal using a new adsorbent [25]. The current study employs RSM to look into the removal of Methyl red dye using a low-cost adsorbent. Statistical designs and surface plots are used for regression analysis and optimization of the removal of colour from aqueous dye solution using a novel adsorbent [26,27]. RSM was used to investigate modelling and optimization for azo dye (Methyl red) degradation using a central composite design [28,29]. The RSM technique can better predict the impact of process variables on performance of those attributes, making it a better optimization alternative [30,31].

In this research, adsorbent was prior treated with Na_2CO_3, which is consistent with the most often used chemical treatment technique for surface treatment of cellulose-based materials, namely alkali treatment to improve sorption capabilities of any adsorbent which is not in activated carbon form [32]. The covalent bond between the components of ligno cellulosic material is also destroyed by treating the jute fibre with an aqueous sodium carbonate (Na_2CO_3) solution, which hydrolyzes depolymerising lignin and hemicellulose. The treatment alters the morphological molecular and super molecular characteristics of cellulose, resulting in changes in pore structure, stiffness, crystallinity accessibility, unit cell structure, and fibril orientation [33]. Washing with Na_2CO_3 improves some of the features of cellulose, such as reactivity, natural ion-exchange capacity, and structural stability. Alkali treatment, which removes waxes and natural lipids from the cellulose fibre surface, identifies some of the chemically reactive functional groups, such as –OH [34]. Rice husk (high in cellulose compounds) treated with alkali (NaOH) has previously seen to be influential as an adsorbent for removing azo dyes from aqueous solutions [35]. Because components like cellulose and hemicellulose are abundant in jute fibres, and Methyl red is essentially an azo dye, the feasibility of employing (alkali treatment) Na_2CO_3 treated jute fibre (NTJF) to remove Methyl red from aqueous solution was investigated in this study.

The goal of this research is to use a mathematical model to analyse the maximum sorption capacity (Q_e) of Na_2CO_3 treated jute fibre (NTJF) in order to eliminate Methyl red (MR), as well as to use response surface methods (RSM) to investigate the effect of process parameters and their performance requirements. The effects of temperature, pH, NTJF dosage, and RPM on adsorption capacity are also investigated using the RSM technique and quantitative mathematical models [31].

After conducting a thorough literature review, the authors discovered that while many studies have been published on the use of adsorption to remove synthetic dyes, no research has been done on the removal of Methyl red dye using modified/treated jute fibre. As a result, the authors have the opportunity to pursue this analysis, which also justifies the novelty of the work.

2. Methods and materials

Jute that had been sun dried naturally was obtained from the market and chopped into 1 mm pieces before being distilled, washed, and dried at 60°C. After that, the sample was treated with 0.01 M Na_2CO_3 for 4 h at 27°C. The sample was then distilled washed to remove any chemicals that were present in excess in the fibre (if any), and the pH was adjusted to 7.0 using 0.1 M NaOH or 0.1 M HCl, before being kept in a container for 24 h after drying at 100°C. The final sample, which was treated with Na_2CO_3 and referred to as treated jute fibre, served as the adsorbent (NTJF). The adsorbate was Methyl red, an azo

dye with the chemical formula $C_{15}H_{15}N_3O_2$ and a molar mass of 269.304 g/mol that has a substantial, but seemingly noncovalent, affinity for cellulose fibres. Analar grade MR dye was obtained from Himedia, To begin the experiment, a stock dye solution (1,000 mg/L; pH 7.0) was made using double distilled water. The chemical structure of Methyl red (MR) is shown in Fig. 1.

2.1. Adsorption capacity and percentage removal

The purpose of the study was to determine the maximum MR sorption capacity (Q_e) of Na_2CO_3 treated jute fibre. Using Eq. (1), the quantity of maximum adsorbed dye per unit adsorbent (milligram (mg) dye adsorbed per gram (g) of adsorbent was derived using the mass balance concept on the concentration of dye:

$$Q_e = \frac{\left(C_i - C_f\right)}{m} V \tag{1}$$

where Q_e = maximum adsorption capacity (mg/g); C_i = dye initial concentration in solution (mg/L); C_f = dye final concentration in solution (mg/L); V = solution volume (L); m = adsorbent weight (g).

The following equation was used to calculate the proportion of dye that was eliminated (%):

$$\text{Dye removal percentage } (\%) = \frac{\left(C_i - C_e\right)}{C_i} \times 100 \tag{2}$$

where C_e = remaining concentration of dye in solution at equilibrium (mg/L).

2.2. Isotherm studies related to sorption

The essential approaches for evaluating the adsorption relationship for adsorbent–adsorbate interaction are studies for various isotherms connected to sorption. Isotherms reveal the homogenous or heterogeneous character of attraction during the adsorbent–adsorbate interaction, as well as adsorption favourability. In this work, the feasibility of MR dye adsorption onto the NTJF was studied using two fundamental non-linear isotherm equations, the Langmuir (1916) and Freundlich (1906) isotherm models, as illustrated in Eqs. (3) and (5), respectively.

$$\text{Langmuir isotherm model: } q_e = \frac{q_m b C_e}{1 + b C_e} \tag{3}$$

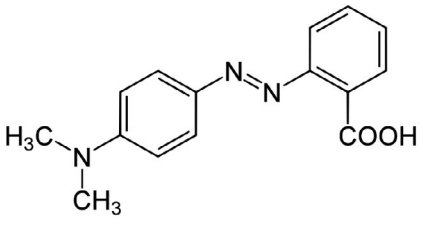

Fig. 1. Molecular structure of Methyl red (MR).

where q_e = dye adsorbed at C_e. (mg/g); q_m = maximum monolayer sorption capacity, not dependent of temperature; b = Langmuir adsorption constant, dependant of temperature (L/mg); C_e = remaining concentration of dye in solution at equilibrium (mg/L).

Upon analysing the value of the unitless constant separation factor (R_L) [36], which can be determined by Eq. (4), suitability of Langmuir model of adsorption can be apprehended. The nature of the isotherm is revealed by the R_L value, which stipulates as to whether the adsorption process is favourable ($R_L < 1$), unfavourable ($R_L > 1$), linear ($R_L = 1$), or irreversible ($R_L = 0$).

$$R_L = \left(\frac{1}{1 + b C_0}\right) \tag{4}$$

where C_0 = initial dye concentration in the solution (mg/L).

The present work examines an empirical equation, the Freundlich [15] isotherm equation, which depicts the diversity of the adsorbent's surface during adsorption.

$$\text{Freundlich: } q_e = K_f C_e^{1/n} \tag{5}$$

where K_f and $1/n$ are system Freundlich abiding attributes; C_e = remaining concentration of dye in solution at equilibrium(mg/L); q_e = adsorption capacity at equilibrium (mg/g).

K_f and n represent the adsorption capacity and intensity, respectively. If K_f value rises as temperature rises, the reaction is said to be endothermic; if K_f value declines as temperature rises, the reaction is said to be exothermic. The other Freundlich constant, $1/n$, indicates the kind of adsorption. When the condition is $0 < 1/n < 1$, the adsorption process is regarded to be favourable; if the condition is $1/n = 1$, the sorption condition should be irreversible; and lastly, if the condition is $1/n > 1$, the adsorption process is considered to be unfavourable [7].

2.3. Adsorption kinetic modelling

The kinetic parameters of the sorption system were then calculated using time-dependent experimental results. The rate constant and optimal sorption capacity at various temperature ranges were estimated using pseudo-first-order [23] and pseudo-second-order [18] kinetic models.

$$\text{Pseudo-first-order: } q_t = q_1\left[1 - \exp\left(-k_1 t\right)\right] \tag{6}$$

$$\text{Pseudo-second-order: } q_t = \frac{q_2^2 k_2 t}{1 + q_2 k_2 t} \tag{7}$$

Because the preceding kinetic models have a constraint when it comes to determining the sorption process' diffusion mechanism, the rate-controlling phases were determined using an intra-particle diffusion model.

$$\text{Intraparticle diffusion: } q_t = k_i t^{0.5} \tag{8}$$

For the sorption of MR onto NTJF, activation energy (E_a) was calculated using the Arrhenius equation. The following is the equation for the same.

$$\ln k = \ln A - \frac{E_a}{RT} \tag{9}$$

The activation energy E_a may be calculated by plotting ln$k$ vs. 1/T on a graph and analysing the slope of the same. Where T is the temperature in kelvin and K is either the pseudo-first-order rate constant or the pseudo-second-order rate constant, and the selection of specific K is based on the kinetic sorption rate preference. Activation energy reveals the nature of adsorption (physical or chemical). To determine the adsorption temperature favourability, whether the sorption process is endothermic or exothermic, and whether the sorption process is entropy or enthalpy operated, some thermodynamic parameters were examined, such as ΔG = change in Gibbs free energy, ΔH = change in enthalpy, and ΔS = change in entropy. The analyses were carried out using the equations shown below.

$$\Delta G = -RT \ln K_{\text{ad}} \tag{10}$$

$$K_{\text{ad}} = \frac{C_0 - C_e}{C_e^{\,n}} \tag{11}$$

$$\Delta G = \Delta H - T\Delta S \tag{12}$$

The values of ΔH and ΔS were calculated using the graph of ΔG vs. T, where C_0 denotes the initial dye concentration in the solution and C_e denotes the equilibrium dye concentration in the solution. K_{ad} is the adsorption process' rate constant at equilibrium. Rate kinetic analysis is used to find the n value, which entails deciding which rate model best matches the observed data [4].

2.4. Batch experimental procedure

A stock dye solution of 1,000 mg/L was prepared initially, henceforth, solutions with concentrations 50, 100, 150 and 200 mg/L were calibrated and were considered for the overall analysis. The goal of this study was to fix a dye concentration (say 50 mg/L) and determine the maximal sorption capacity (Q_e) as a function of the pH, NTJF dosage, temperature, and rotational speed input process parameters (RPM). Adsorption analysis was performed batch by batch to investigate the removal of MR dye using the aforementioned procedure parameters. Let's go over the details of the experiment to see how a change in pH affects the final result (Q_e). The pH range used in the study was (3–11). The initial pH was calibrated to 3.0, the initial NTJF dose was 10 g/L, the initial temperature was 293 K, and the rotary shaker was adjusted with a stirring speed of 100 RPM for 200 mL of dye solution with 50 mg/L dye concentration. A rotary incubator was used to regulate the temperature. After that, the solution was allowed to agitate for 5 min each before samples were taken to determine the concentration of the sample solution (after 5, 10, 15 min and so on up to 180 min). After 120 min of agitation, adsorption was no longer time dependent (equilibrium time). The dye concentrations were calculated using UV/VIS spectroscopy absorbance values with maximum absorbance at a wavelength of 425 nm (λ_{max} = 425 nm). The data were then used to compute Q_e (mg/g), the highest quantity of dye adsorbed. Keeping the other process parameters remained constant, comparable experiments were carried out with different pH values. Similarly, when the pH variation study was completed, other parameters were investigated set-wise by modifying the parameter whose effect was to be determined while leaving the other variables constant.

NTJF dose (10, 14 and 18 g/L), temperature (293, 303, and 323 K), and rotational/stirring speed (100, 150, and 200 RPM) were used to evaluate additional parameters. Using 0.1 M HCl or 0.1 M NaOH, pH values were kept in the range of 3–11 for each set of solutions. Experiments were carried out to see if the MR dye could be absorbed by the container walls in the absence of jute. There was no evidence of deterioration or MR dye absorption on container sides. Duplicate tests were run, and mean values were taken into account. All feasible combinations for all process variables were tested using the same set of experiments.

3. Results and discussion

A time degradation curve is shown to highlight the removal of dye from aqueous solution as a function of contact time. It's calculated by tracking the drop in dye concentration caused by the loss of adsorbent from a solution over time. Fig. 2 shows the time degradation curve for removing MR with NTJF at 50 mg/L initial dye concentration, 14 g/L NTJF dosage, pH 7.0, 150 RPM rotational speed and 303 K temperature. Adsorption reaches equilibrium when there is no more significant adsorption of dye onto the adsorbent beyond a specific time point, or when adsorption of dye is no longer a time-dependent process, as shown by the time degradation curve.

As demonstrated in Fig. 2, the rate of adsorption for the adsorbent–adsorbate interaction was fast within the first 20–25 min. Following then, the adsorption rate plummeted. The quick rate of dye removal in the early phases is attributable to the adsorption site availability. The adsorbate–adsorbent interaction became more intense over time, leading in adsorption site saturation as more dye molecules adsorb onto the sites, resulting in a decrease in the number of adsorption sites and, as a result, a decline in sorption. The equilibrium duration for the present research was 120 min, after which the adsorption process was no longer time dependent, similar results were obtained earlier [5].

3.1. Surface morphology and characterization of NTJF

Scanning electron microscopy (SEM) analysis is an important characterization method in adsorption [37]. Using a scanning electron microscope (SEM) (MODEL: JSM-6360, JEOL), the surface characteristics of virgin NTJF and MR dye adsorbed NTJF were examined under the following conditions: resolution: 3 nm in the secondary electron mode, distance of 8 mm, acceleration voltage of 30 KV, accelerating voltage: from 1–30 KV in 1 KV steps, accelerating voltage: from 1–30 KV in 1 KV steps, accelerating voltage: from 1–30 KV in 1 KV steps, accelerating voltage: from 1–30 KV in 1 KV steps, accelerating voltage: from 1 KV–30 K. Fig. 3a depicts virgin NTJF, while Fig. 3c

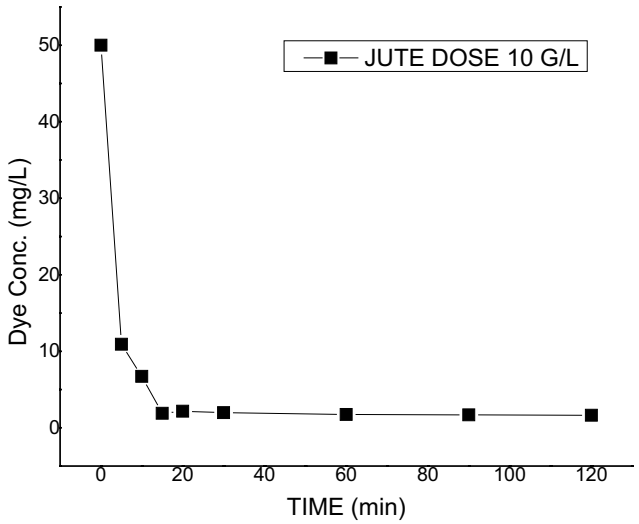

Fig. 2. Time degradation curve for MR sorption onto NTJF.

depicts MR adsorbed NTJF. It can be seen in Fig. 3c that there are numerous MR dye particles attached to the NTJF surface. Both the figures are of 1 μm and ×10,000 resolution. Corresponding energy-dispersive X-ray spectroscopy (EDAX) images are shown in Fig. 3b and d respectively.

Fourier-transform infrared spectroscopy (FTIR) analysis is a useful approach for characterising and recognizing the functional groups accountable for adsorption. The influence of functional groups for the adsorption of MR dye onto adsorbent surfaces is confirmed by the FTIR spectra. FTIR analysis was done at IIT Bombay SAIF research facility. The study's instrument has the following specifications (Make: Bruker, Germany). Model: Hyperion Microscope 3000 with Vertex 80 FTIR System). Fig. 4a and b show the FTIR spectra of virgin NTJF and Methyl red (MR) loaded NTJF, respectively. As in Fig. 4a, due to the constrained hydroxyl or amine groups the broad and strong band was seen at 3,437.84 cm^{-1}. Due to the –CH asymmetric stretching, the next high value of 2,914.16 cm^{-1} was observed. The carboxyl group stretching

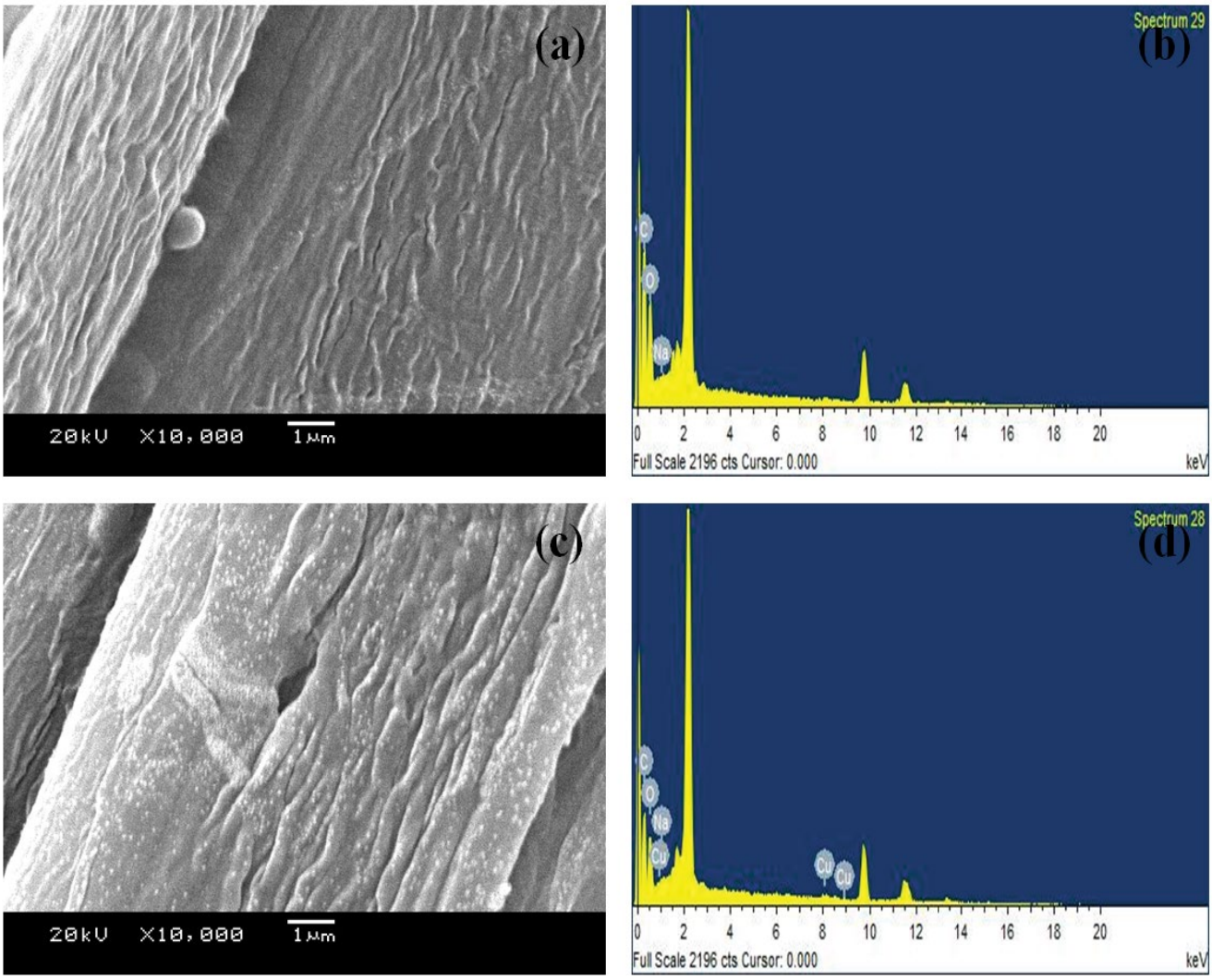

Fig. 3. (a) SEM image of NTJF before adsorption, (b) SEM image of NTJF after MR dye adsorption, (c) EDAX image of NTJF before adsorption and (d) EDAX image of NTJF after MR dye adsorption.

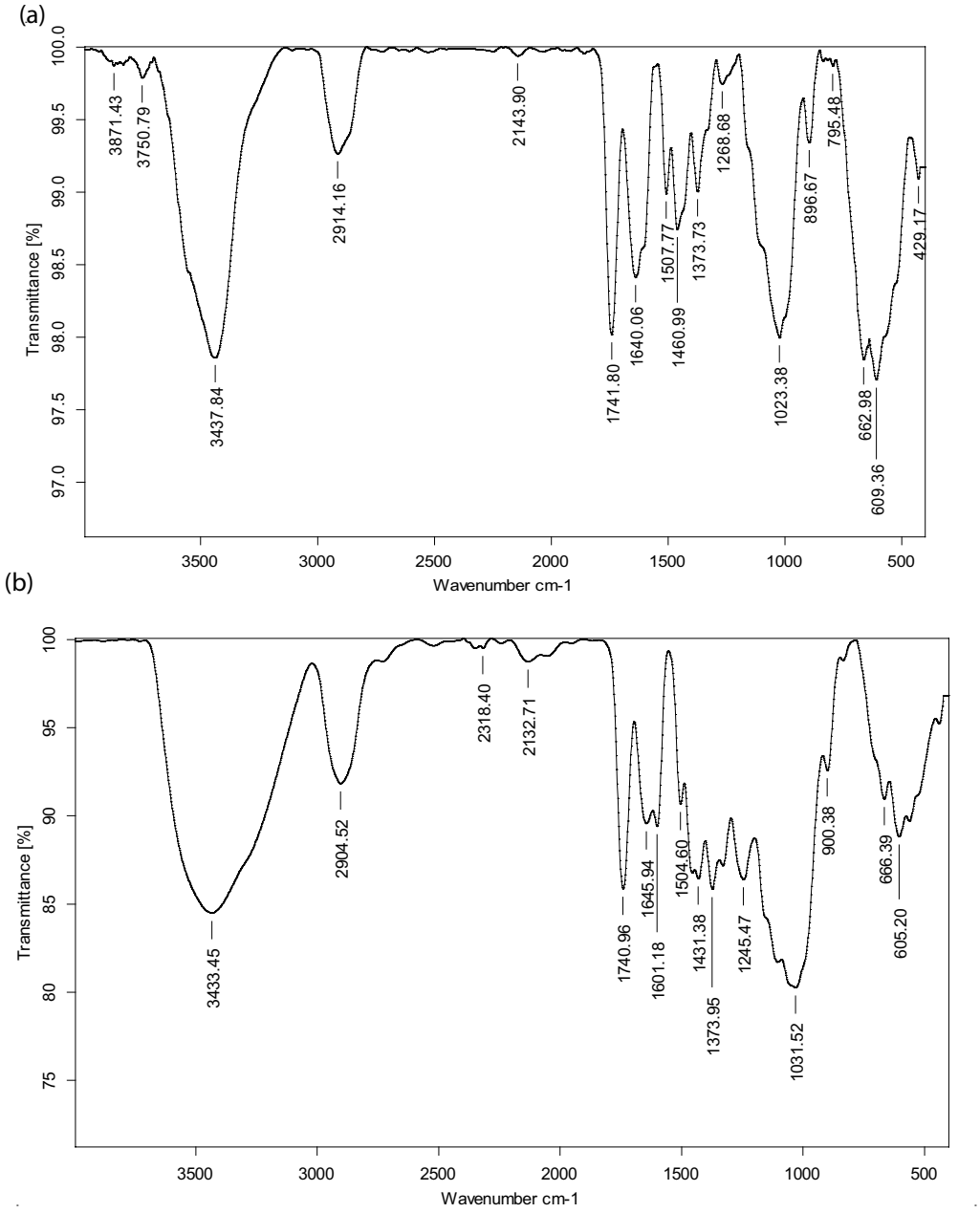

Fig. 4. (a) FTIR spectra of (a) NTJF before adsorption and (b) MR loaded NTJF.

vibration has a wave number of 1,741.80 cm^{-1}. The bands at 1,640.06; 1,507.77 and 1,460.99 cm^{-1} were used to assign asymmetric and symmetric stretching vibrations of C=O groups. At 1,373.73 cm^{-1}, the C–N stretching band was discovered. C–O stretching of alcohols and carboxylic acids was assigned by the band to 1,023.38 cm^{-1}. After MR dye adsorption, as shown in Fig. 4b, the symmetrical stretching vibration bands of hydroxyl or amine groups in MR loaded NTJF were modified from 3,437.84 to 3,433.45 cm^{-1}. The stretching band of carboxyl groups was changed from 1,741.80 to 1,740.96 cm^{-1}, 1,640.06; 1,507.77 and 1,460.99 cm^{-1} stretching bands were likewise changed to 1,645.94; 1,601.18 and 1,431.38 cm^{-1} correspondingly. The C–O peak was moved from 1,023.38 to 1,031.52 cm^{-1}, respectively. Similarly, following adsorption, additional values moved their positions. Thus, it may be inferred that functional groups are the key operators responsible for the binding of MR onto the surface of the NTJF, which is justified according to the examination of FTIR spectra which shows frequency shifts.

3.2. Analysis of batch study parameters

3.2.1. Influence of pH

The point of zero charge is the pH at which an adsorbent surface has a net neutral charge (pH_{pzc}). The importance of

studying pH_{pzc} for any adsorbent is that it exposes the ability of any adsorbent surface to attract anionic or cationic adsorbates. For example, if an adsorbent surface has a positive charge in a solution with a pH lower than pH_{pzc}, the adsorbent surface will attract anionic adsorbates. Similarly, if the adsorbent surface contains a negative charge in a solution with a pH greater than pH_{pzc}, the adsorbent will allure cationic adsorbate [38–40]. Dissociation/ionization, as well as the properties of the sorbent surface and its interaction with adsorbate particles, are all affected by pH [15]. The adsorption process changes as the surface properties of both parties (adsorbent–adsorbate) alter. It was observed in this study that as the pH rises, the Q_e rises as well. Due to electrostatic repulsion, the functional groups on the adsorbent surface are protonated at low pH, leading the absorbent surface to become positively charged, resulting in reduced dye ion adsorption. As the pH of the dye solution rises, so does the adsorption process, since the adsorbent functional groups deprotonate over time, increasing the electrostatic attraction between dye cations and negatively charged sites on the adsorbent. Fig. 5 depicts the influence of pH on dye removal.

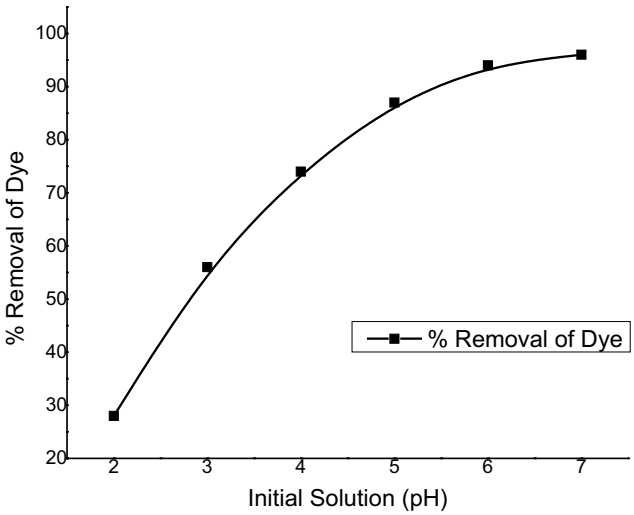

Fig. 5. Percentage removal of MR by NTJF against pH variation.

3.2.2. Influence of adsorbent dose

When evaluating the rate of adsorption capacity of the adsorbate onto the adsorbent surface, one of the important factors to consider is adsorbent dose. The NTJF dosage used in this analysis to determine the adsorption rate ranged from 10 to 18 g/L. There is a substantial increase in dye adsorption and excretion as the NTJF dosage is raised. The increased adsorbent surface area, which increases the number of adsorption sites accessible for adsorption of adsorbates onto the adsorbent, might be the reason for better dye removal rate with a larger NTJF dosage [41]. The same outcome was obtained when the NTJF dosage was raised from 10 to 14.8 g/L. As the NTJF dosage is raised, the absolute adsorption value increases but the adsorption rate drops. The reduction in adsorption rate with a further increase (>14.8 g/L) in NTJF dose may be attributed to particle interaction such as aggregation, which leads to adsorption site saturation, at a constant dye concentration and a constant volume of solution. In addition, we discovered that, while the dye concentration is constant, absorbance is directly proportional to the increase in adsorbent dosage, but adsorption rate is inversely proportional. Fig. 6 shows the effect of NTJF dosage on MR dye elimination percentage.

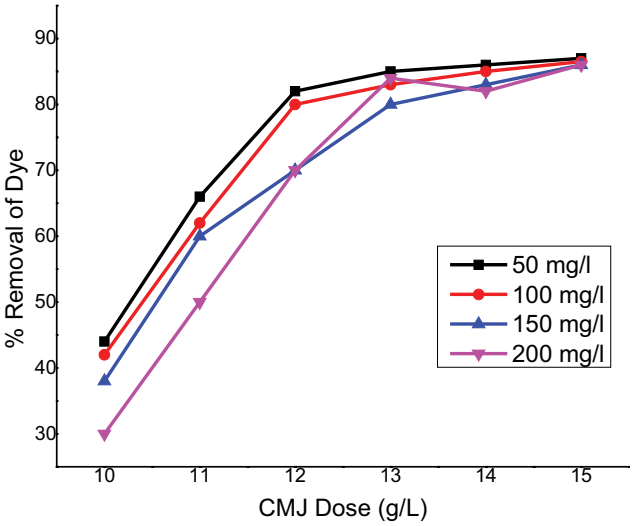

Fig. 6. Percentage removal of dye against NTJF dose.

3.2.3. Influence of temperature

For the reported article, adsorption rate is higher at higher temperatures and vice versa. As the temperature rose, the relationship between adsorbate dye molecules and the adsorbent binding site was stronger [11,12]. This might be due to the fact that temperature influences Methyl red particle diffusion, resulting in a faster mass transfer rate from the bulk to the boundary layer around the jute fibre's surface. It also appears that when the temperature rose, the reaction's speed accelerated. The adsorption capacity of the surface increases as it becomes activated.

3.2.4. Influence of initial concentration of dye

The impact of initial dye concentration on MR adsorption onto Na_2CO_3 treated jute fibre is shown in Fig. 7. A sorbent dosage of 10 mg/L, a temperature of 303 K, and a pH of 7.0 were used in the set's tests. The initial MR dye concentrations in solution were 50, 100, and 150 mg/L, respectively. When the dye concentration was raised from 50 to 150 mg/L for MR adsorption onto Na_2CO_3 treated jute fibre, the sorption percentage decreased from 97.44% to 95.74%. Similar studies have been reported earlier where every rise in dye concentration was accompanied by a drop in % dye clearance. This tendency can be explained by the saturation of sorption sites on the NTJF surface. The formation of a monolayer of dye species on the Jute surface, which reduces the possibility of another layer of dye species accumulating over the monolayer, might explain the decrease in dye removal percentage.

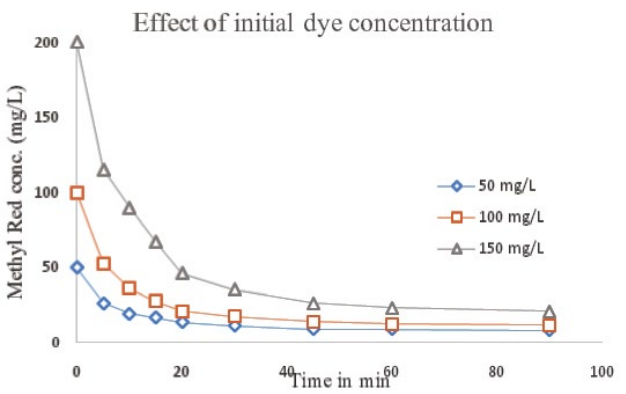

Fig. 7. Influence of initial MR dye concentration onto dye removal capacity.

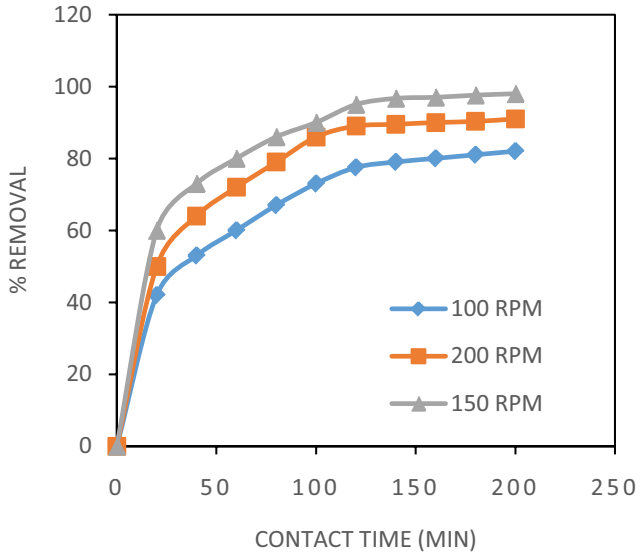

Fig. 8. Percentage removal of dye for different rotational speed (in RPM).

3.2.5. Influence of stirring speed

The stirring/rotational speed has a significant impact on adsorption performance. If the spinning speed (in RPM) is too slow, the adsorbate and adsorbent particles will settle rather than stay suspended. Both the dye and the jute fibres may sink to the bottom of the conical flask used for spinning purposes if the RPM is too low. In order for a prolonged dynamic interaction between them (adsorbent and adsorbate) and, as a result, for adsorption to occur, both sorbent and sorbate must be in suspension [42]. A high rotating speed of the solution lowers the ability of dye particles to settle at the adsorption sites of the adsorbent; instead, a high RPM rate maintains the dye particles floating in the solution, preventing them from settling. Fig. 8 illustrates the effect of stirring/rotational speed.

3.3. Isotherm study

Two nonlinear adsorption isotherms, the Langmuir and Freundlich isotherm investigations, were used to confirm the findings of this study. Fig. 9 displays a plot of the graph of q_e vs. C_e, indicating that the adsorption mechanism better resembles the Langmuir Isotherm, signifying monolayer MR dye adsorption onto the surface of NTJF. Table 1 shows the various isotherm parameters calculated during the investigation at a constant temperature of 303 K.

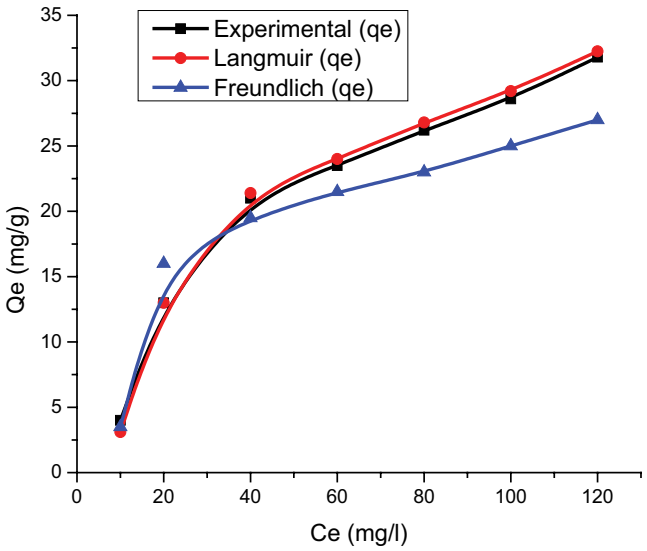

Fig. 9. Adsorption isotherms for MR sorption onto NTJF at 303 K.

3.4. Analysis of rate kinetic models

The rate constants and adsorption equilibrium capacity at various temperatures were determined using two rate kinetic models, pseudo-first-order and pseudo-second-order kinetic sand compared to experimental data. The slopes and intercepts of $\log(q_e - q_t)$ vs. t was used to generate pseudo-first-order rate constants k_1 and q_e. Sorption capabilities found a considerable difference between this kinetic model and theoretical research when comparing theoretical and experimental equilibria of the pseudo-first-order kinetic model. According to the same investigations, experimental data suited the pseudo-second-order kinetic model better. Fig. 10 shows that the pseudo-second-order model matches the experimental data well when compared to the first order kinetic model for the eradication of MR with NTJF.

3.5. Activation energy and thermodynamic parameters

The Arrhenius equation (Eq. (9), section 2.3) and the Arrhenius plot of MR adsorption on NTJF were used to compute the method's activation energy E_a. It was done to figure out what kind of adsorption was going on in the process, and it's crucial for determining if the adsorption is physical or chemical. A low E_a value (40 kJ/mol) indicates physical adsorption, whereas a higher E_a value (40 kJ/mol) indicates chemical adsorption [3]. The graphic was generated with ln$K$ (K = pseudo-second-order rate constant) values in the Y axis and

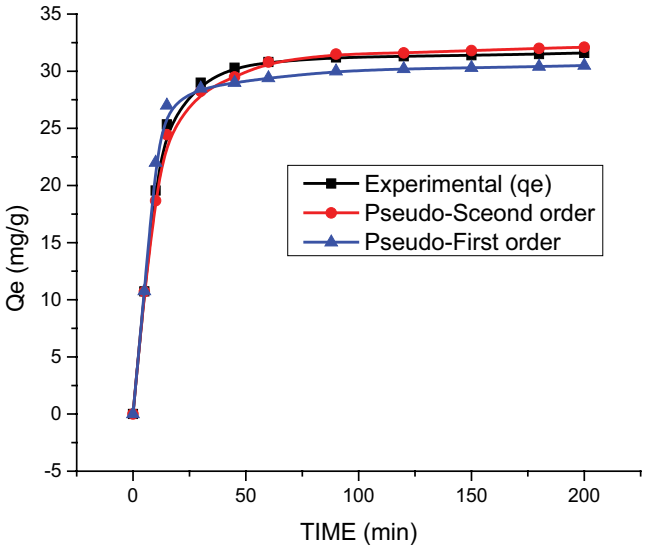

Fig. 10. Adsorption kinetics for MR sorption onto NTJF at 303 K.

1/T (temperature inverse) in the X axis because adsorption rate was better suited to second-order rate constant kinetics in this experiment. From the slope (figure not mentioned) of the linear graph, E_a value is extrapolated as 43.45 kJ/mol, which suggests that chemisorption controls the majority of the ensuing process [3].

The values of the equilibrium rate constant (K_{ad}) were used to estimate one of the thermodynamics parameters, change in Gibb's free energy (ΔG), and the intercepts of the graph of ΔG vs. T (time) were used to determine the other two parameters, entropy (ΔS) and enthalpy (ΔH). The parameters were computed using equations 10, 11, and 12 (section 2.3). For temperature values of 293, 303, and 313 K, ΔG was determined to be –1.84, –5.23, and –9.12 kJ/mol, respectively. The value of change in Gibb's free energy dropped as temperature increased, showing that the adsorption process was appropriate at moderate to high temperatures. The adsorption capacity rose as the temperature increased, meaning that the kinetic energy of the sorbent particles increased. The presence of a positive ΔS value (0.162 kJ/mol K) suggests an entropy-driven increase in randomness at the solid/solution interface. The occurrence of a positive ΔH (12.35 kJ/mol) denotes an endothermic reaction [43–45]. The nature of the adsorption process is determined by the value of ΔH; in general, physical adsorption occurs between 8 and 25 kJ/mol, while chemical adsorption occurs between 80 and 200 kJ/mol [3]. The nature of adsorption is proven to be physical in this investigation by measuring the ΔH value, which validates the study of activation energy. The chemisorption character demonstrated in this study also verifies the activation energy analysis. Various thermodynamic parameters are presented using Table 2.

3.6. Adsorption analysis by adopting response surface methodology

The maximal adsorption capacity (Q_e) was calculated using batch analysis as a function of steering speed (RPM),

Table 1
Several isotherm parameters for MR adsorption onto NTJF

Isotherm model	Parameter	Temperature in Kelvin		
		293 K	303 K	313 K
Langmuir model	Q_e (mg/g)	27.54	32.11	30.95
	b (L/mg)	8.245	8.915	9.312
	R_L	0.019	0.016	0.025
	R^2	0.987	0.998	0.998
Freundlich model	K_f (mg/g)	11.56	11.96	12.87
	n	5.34	6.78	7.13
	R^2	0.934	0.949	0.941

Table 2
Parameters from thermodynamics for MR sorption onto NTJF

Parameters	Temperature in Kelvin		
	293 K	303 K	313 K
ΔG (kJ/mol)	–1.84	–5.23	–9.12
ΔS (kJ/mol K)		0.162	
ΔH (kJ/mol)		12.35	

NTJF dosage (g/L), pH and temperature (K). Several Q_e values were evaluated in a series by changing one of the process parameters while keeping the others constant. Similarly, Q_e values were obtained 30 times utilising the response surface approach by performing 30 alternative sets of process parameter combinations, which were then utilised to find the most desirable state. RSM (response surface methodology) is a statistical and mathematical tool for optimising and modelling quantitative independent aspects in response characteristics. A regression model, also known as a polynomial quadratic model of order two, describes the system quality characteristic, as illustrated in equation 13 [30]. The regression model's coefficient is evaluated using the modelling tool "Design Expert 11.0".

$$Y = C_0 + \sum_{i=1}^{n} C_i X_n + \sum_{i=1}^{n} d_i X_i^2 \pm \varepsilon \tag{13}$$

The face cantered central composite second-order design (CCD) method was predominantly used in the current study's experimental design. When all variables are combined at two levels (high, +1, and low, –1) the CCD full factorial design, which contains eight-star points and six centre points (coded level 0), corresponds to α (alpha) value of 1. 30 trials with four process variables make up the 'face centred CCD'. The proper range of process parameters, as well as their coded and real values, are shown in Table 3. Table 4 shows the coded form of the experimental design architecture employed in this investigation.

When compared to Q_e's statistical analysis, the model fit summary revealed that the second-order quadratic model had a lot of significance. Table 5 shows the results of the quadratic model investigation using analysis of variance (ANOVA). The model F-value indicates how important

the model is. The likelihood that the F value for the model's term is more than 0.95 (i.e., = 0.05, or 95% confidence) indicates that the model generated should be statistically significant and required, since it implies that the model terms influence performance attributes [20]. The response models fit the real data better when the multiple coefficients of regression R^2 are near to unity. The gap between real and anticipated values narrows considerably. The degree of proximity is shown in Fig. 11, which illustrates a graph between the actual and expected response levels (Q_e). The majority of the data points are close to a straight line, indicating that the errors were distributed in a predictable manner. The value of appropriate precision (AP) for the suggested regression model, as defined by ANOVA, was greater than 3 in this experiment. With the use of AP, the predicted value span at the design point is compared to the mean prediction error to see if the model discrimination is enough. The coefficients of determination (R^2) have a higher value in the generated model, and the precision is suitable. R^2 = 0.95 and AP = 14.68 were the results of the provided study for Q_e. As a consequence, the constructed quadratic mathematical model has a significant influence on fitting and forecasting observational findings, but the lack-of-fit test has no bearing (Table 5). The backward elimination approach was used to eliminate insignificant/insignificant components

Table 3
Experimental operating parameters with range of levels

Parameters	Factors	Levels		
		–1	0	+1
pH	*A*	3	7	11
Temperature, (°K)	*B*	293	303	313
NTJF dose, (g/L)	*C*	10	14	18
Rotational speed, (RPM)	*D*	100	150	200

Table 4
Design layout and experimental results

Exp. no.	Factor 1 *A*: pH	Factor 2 *B*: Temp.	Factor 3 *C*: NTJF dose	Factor 4 *D*: RPM	Response Q_e (mg/g)
1	3	313	10	200	10.21
2	3	293	10	100	11.42
3	11	293	18	200	15.67
4	3	313	10	100	5.19
5	11	313	18	100	10.43
6	3	313	18	200	12.69
7	3	293	10	200	11.76
8	11	293	10	200	11.28
9	7	303	14	150	31.91
10	11	313	10	200	11.19
11	11	313	10	100	11.01
12	7	303	14	150	30.98
13	7	303	14	150	31.56
14	3	293	18	100	12.64
15	3	293	18	200	16.34
16	11	313	18	200	13.41
17	11	293	10	100	11.29
18	11	293	18	100	13.38
19	3	313	18	100	11.31
20	7	303	14	150	30.59
21	7	303	14	150	32.11
22	7	303	14	150	31.89
23	7	303	14	100	28.48
24	3	303	14	150	24.91
25	7	303	10	150	27.21
26	7	293	14	150	28.29
27	7	313	14	150	27.28
28	7	303	14	200	26.19
29	7	303	18	150	29.56
30	11	303	14	150	27.87

Table 5
ANOVA results for Q_e

Source	Sum of squares	df	Mean square	*F*-value	*p*-value	Remark
Model	2,241.69	14	160.12	29.34	<0.0001	significant
A-pH	4.56	1	4.56	0.8356	0.3751	
B-Temperature	22.38	1	22.38	4.10	0.0610	
C-NTJF dose	40.11	1	40.11	7.35	0.0161	
D-RPM	15.29	1	15.29	2.80	0.1149	
AB	3.22	1	3.22	0.5904	0.4542	
AC	2.46	1	2.46	0.4517	0.5118	
AD	1.56	1	1.56	0.2863	0.6004	
BC	0.2601	1	0.2601	0.0477	0.8301	
BD	0.6561	1	0.6561	0.1202	0.7336	
CD	1.45	1	1.45	0.2661	0.6135	
A^2	132.43	1	132.43	24.27	0.0002	
B^2	13.64	1	13.64	2.50	0.1348	
C^2	44.71	1	44.71	8.19	0.0119	
D^2	84.31	1	84.31	15.45	0.0013	
Residual	81.86	15	5.46			
Lack of fit	81.25	10	8.12	66.67	0.114	Insignificant
Pure error	0.6093	5	0.1219			
Cor. total	2,323.55	29				

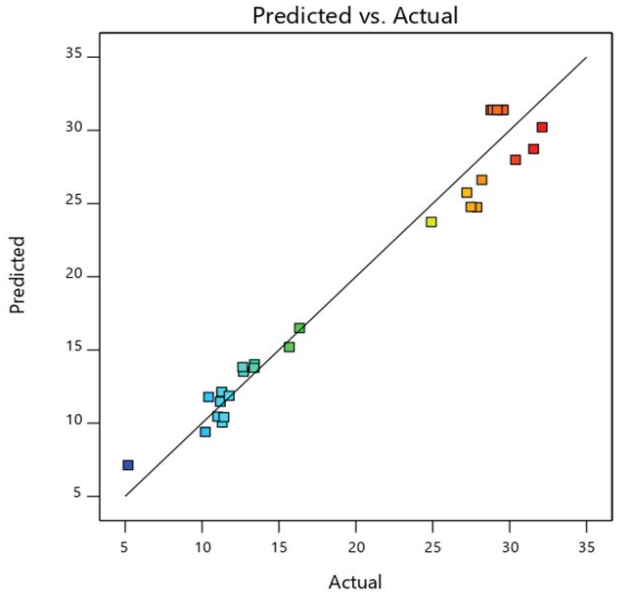

Fig. 11. Predicted vs. actual plot for Q_e.

from the fitted quadratic response surface models in order to localise them. When the inconsequential quadratic model terms are eliminated, the lack of fit test is judged to be unimportant. As illustrated in Fig. 12, multiple response surface graphs were constructed for the same goal of analysing Q_e under various operating conditions. The approximated response surface plot for Q_e in relation to solution process parameters such as pH, NTJF dosage, Temperature, and rotational speed (in RPM) is shown in Fig. 12a–c.

3.7. Multi response optimization based on desirability criteria

Table 6 provides the objectives and ranges for operating process variables such as steering speed (RPM), pH, temperature and NTJF dose as well as the response parameter Q_e. The goal of the RSM technique is to identify a set of optimal operating conditions that will aid in achieving the primary goal. The 1.0 desirability value is not an absolute need because it is purely decided by how near the upper and lower boundaries are found to be set relative to the true optimum.

For the provided design space limits for Q_e, statistical design expert software 11.0 is used to develop an optimum solution consisting of 30 sets. The ideal processing condition for the desired performance characteristics is chosen from a set of parametric conditions with the highest desirability value [46,47]. The optimum parametric condition with the highest desire function is shown in Table 7. The identification and verification of the augmentation of response characteristics by applying the optimal level of processing parameters is the ultimate measure after the perfect set of input parameters has been discovered. To investigate and compare with the ideal value of response characteristics, a confirmation test was performed at the optimal setting of process parameter for steering speed (RPM), temperature, NTJF dose and pH. Table 8 shows the error percentage acquired for experimental validation of the response models developed using the best process parameter setting at the time of experimentation. As per table, percentage error is 1.2 which is quite small.

Figs. 13 and 14 use a graph of a ramp function and a bar graph, respectively, to depict the desirability function for performance qualities [48]. Each dot on the ramp represents the parameter values or response estimate for each

Table 6
Desirability responses based on range of input parameters

Name	Goal	Lower Limit	Upper Limit	Lower Weight	Upper Weight	Importance
A:pH	is in range	3	11	1	1	3
B:Temperature	is in range	293	313	1	1	3
C: NTJF dose	is in range	10	18	1	1	3
D:RPM	is in range	100	200	1	1	3
Q_e	maximize	5.19	32.11	1	1	3

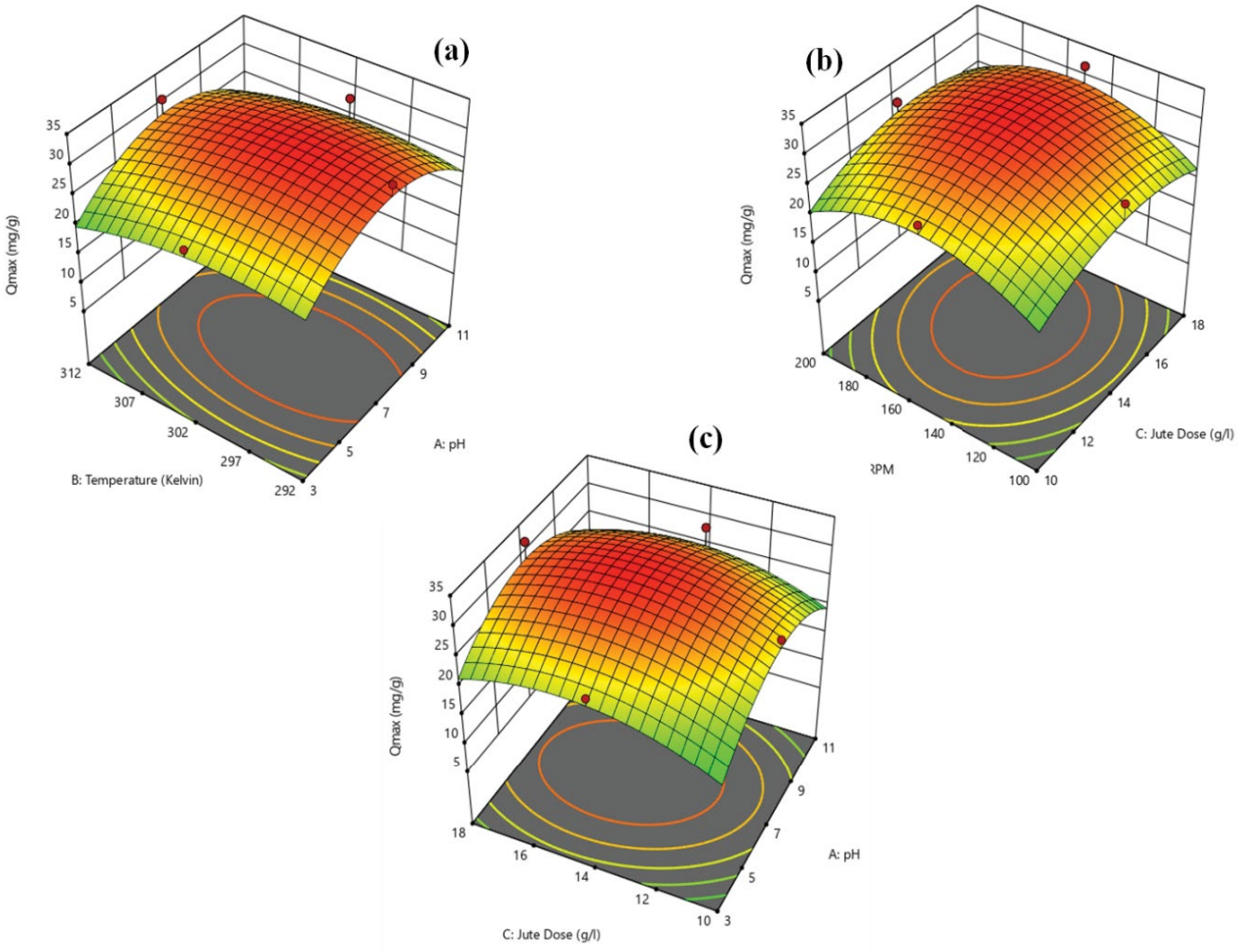

Fig. 12. Q_e response surface plot, (a) temperature vs. pH, (b) RPM vs. NTJF dose and (c) NTJF dose vs. pH.

Table 7
Optimum values depending upon input operating parameters

Parameter	Goal	Optimum value
pH	in range	7.1
Temperature, (°K)	in range	299.56
NTJF dose, (g/L)	in range	14.7
Rotational speed, (RPM)	in range	154

Table 8
Q_e responses, predicted and experimental values

Responses	Q_e (mg/g)
Goal	Maximize
Predicted value	31.7
Experimental value	32.11
Error (%)	1.2

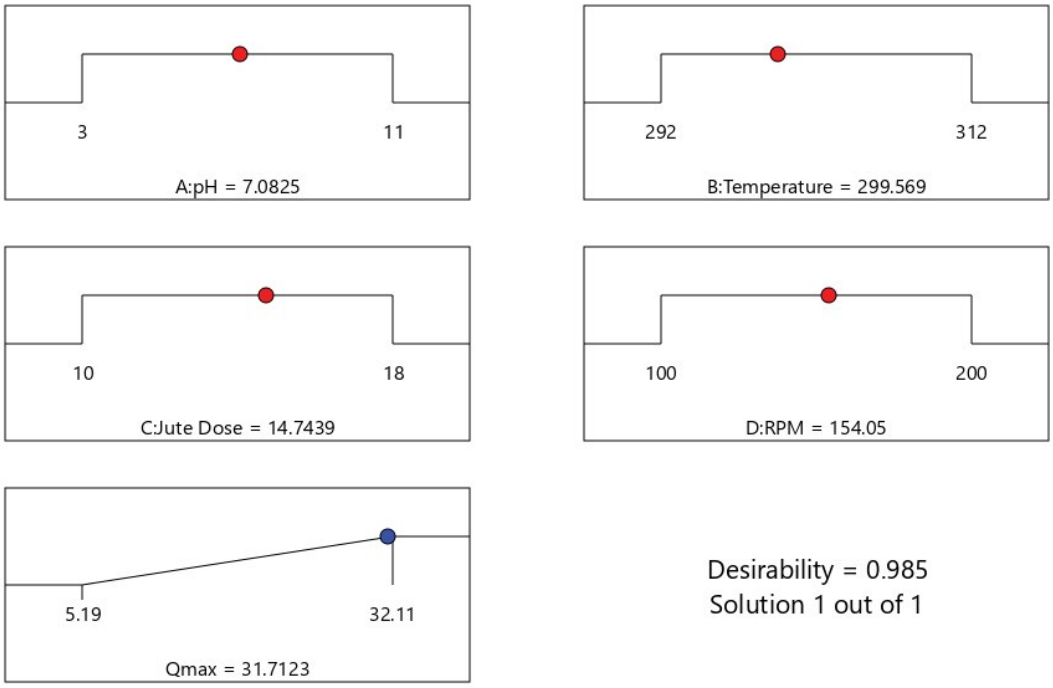

Fig. 13. Ramp function plot of desirability for Q_e.

performance characteristic. The dot's height indicates the reaction's desirability level. Between the objective and the high value, or between the target and the high value, a linear ramp function is constructed, with the value of each weight component equal to one [49]. A bar graph is used to assess the function of overall desirability of quality behaviours. Depending on how near the response is to the objective, the value of desirability varies from 0 to 1. The bar graph shows how well each process variable matches the design requirement, with values around one indicating good fit.

A Q_e 3D desire graph was developed using process parameters in range and maximum response characteristics. Fig. 15 shows the distribution of the desirability function for the predicted response of Q_e inconsonance to temperature and pH. The ideal desirability zone was discovered around the top of the plot, where the overall desirability value was more than 0.98, and steadily decreased as the plot travelled right and backwards. As a consequence, the response's proximity to the objective is shown by the disclosed desirability value of 0.98 [50–52].

3.8. Adsorption mechanism

One of the most exciting elements of any adsorption study is deciphering the process of adsorption. To do so, two factors are critical: (1) the adsorbate structure, and (2) the adsorbent's functional groups that are responsible for adsorption. In the present analysis, amino groups present in MR dye molecules formed hydrogen bonds with the exposed hydroxyl groups in NTJF [22–24] and this bonding is the primary reason for adsorption. According to the findings of SEM and FTIR experiments, treating jute fibre with Na_2CO_3 changes the surface morphology, decreases the silica content, and enhances the crystallinity of the cellulose fraction. Part 2 of this article delves into the subject in depth. This change in surface characteristics of treated jute fibre would likely favour chemical reaction between the hydroxyl groups exposed adsorbent and dye ions, as well as mechanical bonding, because dye ions are better attached to the altered and suitable adsorbent molecular structure [53].

All of the trials exhibited a high rate of adsorption for the first 20–25 min, which subsequently slowed down gradually until the equilibrium time was achieved at 120 min, showing that intra-particle diffusion was dominant and aided by film diffusion. The NTJF dosage and RPM were critical determinants in determining sorption capacity, which was highest at pH 7.0. Based on the observations, the following adsorption mechanism may be inferred:

- The MR dye is transferred from the solution to the jute fibre's surface.
- Dye molecule adsorption on the surface of jute fibres is assumed to be caused by the establishment of a hydrogen bond between the dye's amino groups and the exposed hydroxyl group in the jute fibres.
- Dye particles diffuse from the aqueous solution to the adsorbent surface through the boundary layer.

3.9. Use of non-carbon adsorbents for MR dye removal

Table 9 shows the findings of a comparative investigation for the removal of MR dye using several non-carbon based adsorbents. All of the adsorbents employed in the

Table 9
MR dye removal using various non-carbon based adsorbent

Sl. no	Type of adsorbent	Maximum adsorption capacity (Q_e)	Reference
1	Modified coconut husk	71 mg/g	[54]
2	Water hyacinth (*Eichhornia crassipes*) biomass	8.85×10^{-2} mol/g	[55]
3	White potato peel powder	30.48 mg/g	[56]
4	Natural and purified organic matter rich clay	397 mg/g	[57]
5	Banana pseudostem fibers	96.39%	[58]
6	Bentonite type clay from Mostaganem region (MBC)	2 mg/g	[59]
7	Shell of the cocoa pod	6.39–13.88 mg/g	[60]
8	Eggshell powder (ESP)	1.66 mg/g	[61]
9	Na_2CO_3 modified jute fibre	32.11 mg/g	This study

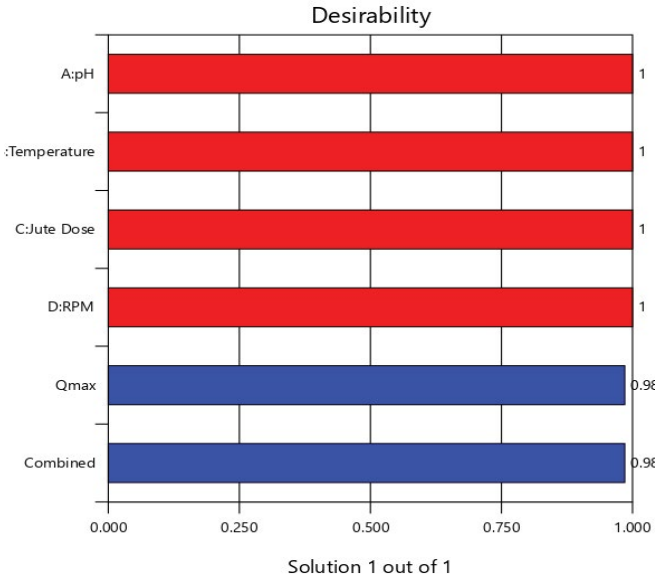

Fig. 14. Bar graph of desirability Q_e.

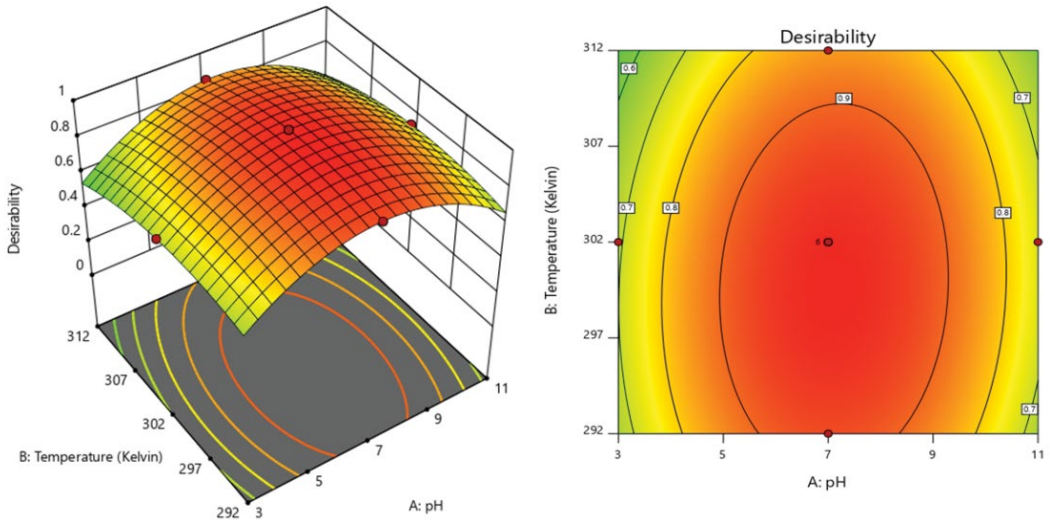

Fig. 15. 3D surface plot of desirability of Q_e for temperature and pH.

analysis were changed from agricultural waste or other types of modified adsorbents.

4. Conclusions

The feasibility and efficiency of removing an anionic azo dye, Methyl red (MR), utilising chemically (Na_2CO_3) treated jute fibre by adsorption technology were investigated using the face-centred central (CCD) response surface paradigm in composite design. The effect of input process/operating parameters such as NTJF dose, pH, Temperature, and stirring speed was successfully investigated for designing the output of maximum adsorption capacity by participating in 30 experimental trials with three repetitions in each of the process parameters at three different levels. The results of the modelling reveal that moderate to high NTJF dose, moderate RPM, moderate to high temperature, and neutral pH are necessary for optimum adsorption capacity within the examined range of operational parameters. The R^2 value of 0.98 for Q_e validates this, indicating the model's suitability. The NTJF dose and pH were two important elements that determined the result of Q_e. The impact of each process parameter and its reasons are addressed in the various sections of this article. Rotational speed 154 RPM, temperature 299.56 K, NTJF dose 14.74 mg/L, and pH 7.08 were the optimal parameter values for maximising Q_e. The satisfactory error percentage of 1.2 between the expected and actual values for Q_e confirms the methodology's accuracy.

Author contributions

This is to state that: A.K.D. (Assistant professor) did the experimental study, analyses and wrote the manuscript. A.D. (Assistant Professor) worked on the use of mathematical modelling of the experimental works. And R.G. (Ph.D. Scholar) wrote and revised the manuscript.

References

[1] C. Arora, S. Soni, P.K. Bajpai, J. Mittal, A. Mariyam, Dye Removal from Waste Water Using Metal Organic Frameworks, in: Management of Contaminants of Emerging Concern (CEC) in Environment, 2021, pp. 375–394.

[2] A.K. Dey, U. Kumar, Adsorption of anionic azo dye Congo red from aqueous solution onto NaOH-modified jute fibre, Desal. Water Treat., 92 (2017) 301–308.

[3] J. Mittal, Permissible synthetic food dyes in India, Resonance – J. Sci. Educ., 25 (2020) 567–577.

[4] A.K. Dey, U. Kumar, A. Dey, Use of response surface methodology for the optimization of process parameters for the removal of Congo red by NaOH treated jute fibre, Desal. Water Treat., 115 (2018) 300–314.

[5] A.K. Dey, A. Dey, Selection of optimal processing condition during removal of Reactive Red 195 by NaOH treated jute fibre using adsorption, Groundwater Sustainable Dev., 12 (2021) 100522, doi: 10.1016/j.gsd.2020.100522.

[6] O. Aksakal, H. Ucun, Equilibrium, kinetic and thermodynamic studies of the biosorption of textile dye (Reactive Red 195) onto *Pinus sylvestris* L., J. Hazard. Mater., 181 (2010) 666–672.

[7] A.K. Dey, U. Kumar, Adsorption of Reactive red 195 from polluted water upon Na_2CO_3 modified jute fibre, Int. J. Eng. Technol., 9 (2017) 53–58.

[8] S. Chatterjee, A. Kumar, S. Basu, S. Dutta, Application of response surface methodology for Methylene blue dye removal from aqueous solution using low cost adsorbent, Chem. Eng. J., 181–182 (2012) 289–299.

[9] Y. Chen, D. Zhang, Adsorption kinetics, isotherm and thermodynamics studies of flavones from *Vaccinium Bracteatum Thunb* leaves on NKA-2 resin, Chem. Eng. J., 254 (2014) 579–585.

[10] A.K. Dey, A. Dey, R. Goswami, Fixed-bed column analysis for adsorption of Acid scarlet 3R dye from aqueous solution onto chemically modified betel nut husk fibre, Desal. Water Treat., 252 (2022) 381–390.

[11] I.-H. Cho, K.-D. Joh, Photocatalytic degradation of azo dye (*Reactive red 120*) in TiO_2/UV system: optimization and modeling using a response surface methodology (RSM) based on the central composite design, Dyes Pigm., 75 (2007) 533–543.

[12] M.N. Chong, B. Jin, C.W.K. Chow, C.P. Saint, A new approach to optimize an annular slurry photoreactor system for the degradation of Congo red: statistical analysis and modelling, Chem. Eng. J., 152 (2009) 158–166.

[13] S. Chowdhury, R. Mishra, P. Saha, P. Kushwaha, Adsorption thermodynamics, kinetics and isosteric heat of adsorption of malachite green onto chemically modified rice husk, Desalination, 265 (2011) 159–168.

[14] S. Chowdhury, P. Saha, Sea shell powder as a new adsorbent to remove Basic green 4 (Malachite green) from aqueous solutions: equilibrium, kinetic and thermodynamic studies, Chem. Eng. J., 164 (2010) 168–177.

[15] D. Harikishore Kumar Reddy, Y.-S. Yun, Spinel ferrite magnetic adsorbents: alternative future materials for water purification?, Coord. Chem. Rev., 315 (2016) 90–111.

[16] G. Crini, H.N. Peindy, F. Gimbert, C. Robert, Removal of C.I. Basic green 4 (Malachite green) from aqueous solutions by adsorption using cyclodextrin-based adsorbent: kinetic and equilibrium studies, Sep. Purif. Technol., 53 (2007) 97–110.

[17] H.M.F. Freundlich, Over the adsorption in solution, J. Phys. Chem., 57 (1906) 385–471.

[18] P.K. Ganguly, S. Chanda, Dyeing of jute: effect of progressive removal of hemicellulose and lignin, Indian J. Fibre Text. Res., 19 (1994) 38–41.

[19] M. Maqbool, H.N. Bhatti, S. Sadaf, M.M. AL-Anazy, M. Iqbal, Biocomposite of polyaniline and sodium alginate with *Oscillatoria* biomass: a potential adsorbent for the removal of Basic blue 41, J. Mater. Res. Technol., 9 (2020) 14729–14741.

[20] V.S. Munagapati, D.-S. Kim, Adsorption of anionic azo dye Congo red from aqueous solution by cationic modified orange peel powder, J. Mol. Liq., 220 (2016) 540–548.

[21] V.K. Gupta, D. Pathania, S. Sharma, S. Agarwal, P. Singh, Remediation and recovery of methyl orange from aqueous solution onto acrylic acid grafted *Ficus carica* fiber: isotherms, kinetics and thermodynamics, J. Mol. Liq., 177 (2013) 325–334.

[22] Y.S. Ho, G. McKay, Pseudo-second-order model for sorption processes, Process Biochem., 34 (1999) 451–465.

[23] S. Ibrahim, I. Fatimah, H.-M. Ang, S. Wang, Adsorption of anionic dyes in aqueous solution using chemically modified barley straw, Water Sci. Technol., 62 (2010) 1177–1182.

[24] H.K. Kansal, S. Singh, P. Kumar, Technology and research developments in powder mixed electric discharge machining (PMEDM), J. Mater. Process. Technol., 184 (2007) 32–41.

[25] I.K. Kapdan, R. Ozturk, Effect of operating parameters on color and COD removal performance of SBR: sludge age and initial dyestuff concentration, J. Hazard. Mater., 123 (2005) 217–222.

[26] M. Koch, A. Yediler, D. Lienert, G. Insel, A. Kettrup, Ozonation of hydrolyzed azo dye reactive yellow 84 (CI), Chemosphere, 46 (2002) 109–113.

[27] S. Lagergren, About the theory of so-called adsorption of soluble substances, Kungliga Svenska Vetenskapsakademiens, Handlingar, Band, 24 (1898) 1–39.

[28] I. Langmuir, The constitution and fundamental properties of solids and liquids. Part I. Solids, J. Am. Chem. Soc., 38 (1916) 2221–2295.

[29] S. Liang, X. Guo, N. Feng, Q. Tian, Isotherms, kinetics and thermodynamic studies of adsorption of Cu^{2+} from aqueous solutions by Mg^{2+}/K^+ type orange peel adsorbents, J. Hazard. Mater., 174 (2010) 756–762.

[30] Y. Liu, Y.-J. Liu, Biosorption isotherms, kinetics and thermodynamics, Sep. Purif. Technol., 61 (2008) 229–242.
[31] A.K. Dey, A. Dey, Selection of Optimal Processing Condition During Removal of Methylene Blue Dye Using Treated Betel Nut Fibre Implementing Desirability Based RSM Approach, P. Kayaroganam, Ed., Response Surface Methodology in Engineering Science, 2021, doi: 10.5772/intechopen.98428.
[32] V.S. Munagapati, D.-S. Kim, Adsorption of anionic azo dye Congo red from aqueous solution by cationic modified orange peel powder, J. Mol. Liq., 220 (2016) 540–548.
[33] T.Y. Mustafa, T.K. Sen, S. Afroze, H.M. Ang, Dye and its removal from aqueous solution by adsorption: a review, Adv. Colloid Interface Sci., 209 (2014) 172–184.
[34] C. Namasivayam, M.V. Sureshkumar, Anionic dye adsorption characteristics of surfactant-modified coir pith, a 'waste' lignocellulosic polymer, J. Appl. Polym. Sci., 100 (2006) 1538–1546.
[35] B.S. Ndazi, C. Nyahumwa, J.V. Tesha, Chemical and thermal stability of rice husks against alkali treatment, BioResources, 3 (2007) 1267.
[36] T. Panswad, S. Wongchaisuwan, Mechanisms of dye wastewater colour removal by magnesium carbonate-hydrated basic, Water Sci. Technol., 18 (1986) 139–144.
[37] M. Maqbool, S. Sadaf, H.N. Bhatti, S. Rehmat, A. Kausar, S.A. Alissa, M. Iqbal, Sodium alginate and polypyrrole composites with algal dead biomass for the adsorption of Congo red dye: kinetic, thermodynamics and desorption studies, Surf. Interfaces, 25 (2021) 101183, doi: 10.1016/j.surfin.2021.101183.
[38] K. Ravikumar, S. Krishnan, S. Ramalingam, K. Balu, Optimization of process variables by the application of response surface methodology for dye removal using a novel adsorbent, Dyes Pigm., 72 (2007) 66–74.
[39] K. Ravikumar, B. Deebika, K. Balu, Decolourization of aqueous dye solutions by a novel adsorbent: application of statistical designs and surface plots for the optimization and regression analysis, J. Hazard. Mater., 122 (2005) 75–83.
[40] T.W. Webi, R.K. Chakravorty, Pore and solid diffusion models for fixed-bed adsorbents, AICHE J., 20 (1974) 228–238.
[41] B. Railsback, Some Fundamentals of Mineralogy and Geochemistry, Dept. of Geology, Univ. of Georgia, Athens, GA, 2006.
[42] D.H. Lataye, I.M. Mishra, I.D. Mall, Removal of pyridine from aqueous solution by adsorption on bagasse fly ash, Ind. Eng. Chem. Res., 45 (2006) 934–3943.
[43] D.H. Lataye, I.M. Mishra, I.D. Mall, Multicomponent sorptive removal of toxics pyridine, 2-picoline, and 4-picoline from aqueous solution by bagasse fly ash: optimization of process parameters, Ind. Eng. Chem. Res., 47 (2008) 5629–5635.
[44] A. Saeed, M. Sharif, M. Iqbal, Application potential of grapefruit peel as dye sorbent: kinetics, equilibrium and mechanism of crystal violet adsorption, J. Hazard. Mater., 179 (2010) 564–572.
[45] M.T. Yagub, T.K. Sen, H. Ang, Equilibrium, kinetics, and thermodynamics of methylene blue adsorption by pine tree leaves, Water Air Soil Pollut., 223 (2012) 5267–5282.
[46] J. Vadiveloo, B. Nurfariza, J.G. Fadel, Nutritional improvement of rice husks, Animal Feed Sci. Technol., 151 (2009) 299–305.
[47] T.A. El-Taweel, Multi-response optimization of EDM with Al–Cu–Si–TiC P/M composite electrode, Int. J. Adv. Manuf. Technol., 44 (2009) 100–113.
[48] T.A. El-Taweel, S.A. Gouda, Performance analysis of wire electrochemical turning process—RSM approach, Int. J. Adv. Manuf. Technol., 53 (2011) 181–190.
[49] M. Rahman, A. Dey, K.M. Pandey, Machinability of cenosphere particulate–reinforced AA6061 aluminium alloy prepared by compocasting, Proc. Inst. Mech. Eng., Part B: J. Eng. Manuf., 232 (2018) 2499, doi: 10.1177/0954405417699013.
[50] A. Dey, K.M. Pandey, Selection of optimal processing condition during WEDM of compocasted AA6061/cenosphere AMCs based on grey-based hybrid approach, Mater. Manuf. Processes, 33 (2018) 1549–1558.
[51] A. Dey, M. Debnath, K.M. Pandey, Analysis of effect of machining parameters during electrical discharge machining using Taguchi-based multi-objective PSO, Int. J. Comput. Intell. Appl., 16 (2017) 1750010, doi: 10.1142/S1469026817500109.
[52] A. Dey, K.M. Pandey, Wire electrical discharge machining characteristics of AA6061/cenosphere as-cast aluminum matrix composites, Mater. Manuf. Processes, 33 (2018) 1346–1353.
[53] Y. Su, B. Zhao, W. Xiao, R. Han, Adsorption behavior of light green anionic dye using cationic surfactant-modified wheat straw in batch and column mode, Environ. Sci. Pollut. Res., 20 (2013) 5558–5568.
[54] E.A. Aziz, A.S. Abdul Razak, S. Sulaiman, H.A. Halim, M.S. Islam, N.A. Zainodin, W.A. Wan Omar, The performance of coconut husk and shell for the removal of Methyl red from aqueous solution: adsorption equilibrium and kinetic study, J. Eng. Appl. Sci., 11 (2016) 2500–2507.
[55] T. Tarawou, M. Horsfall Jr., J.L. Vicente, Adsorption of Methyl red by water-hyacinth (*Eichornia crassipes*) biomass, Chem. Biodivers., 4 (2007) 2236–2245.
[56] C.K. Enenebeaku, N.J. Okorocha, E.E. Uchechi, I.C. Ukaga, Adsorption and equilibrium studies on the removal of Methyl red from aqueous solution using white potato peel powder, Int. Lett. Chem. Phys. Astron., 72 (2017) 52–64.
[57] D.F. Romdhane, Y. Satlaoui, R. Nasraoui, A. Charef, R. Azouzi, Adsorption, modeling, thermodynamic, and kinetic studies of Methyl red removal from textile-polluted water using natural and purified organic matter rich clays as low-cost adsorbent, J. Chem., 2020 (2020) 4376173, doi: 10.1155/2020/4376173.
[58] Z. Yet, M.Z.A. Rahim, Removal of Methyl red from aqueous solution by adsorption on treated banana pseudostem fibers using response surface method (RSM), Malaysian J. Anal. Sci., 18 (2014) 592–603.
[59] K. Boudouara, M. Ghelamallah, H.N. Khemliche, Adsorption of Methyl red from Aqueous Solutions by Algerian Bentonite Clay, 2nd International Congress on Energy Efficiency and Energy Related Materials, Springer, Cham, 2014, pp. 203–209.
[60] R. Lafi, L. Abdellaoui, L. Montasser, W. Mabrouk, A. Hafiane, The effect of head group of surfactant on the adsorption of Methyl red onto modified coffee residues, J. Mol. Struct., 1249 (2022) 131527, doi: 10.1016/j.molstruc.2021.131527.
[61] S. Rajoriya, V.K. Saharan, A.S. Pundir, M. Nigam, K. Roy, Adsorption of Methyl red dye from aqueous solution onto eggshell waste material: kinetics, isotherms and thermodynamic studies, Curr. Res. Green Sustainable Chem., 4 (2021) 100180, doi: 10.1016/j.crgsc.2021.100180.